PHYSICAL REVIEW B **87**, 224502 (2013)

$Y_3Pt_4Ge_{13}$: A superconductor with a noncentrosymmetric crystal structure

Roman Gumeniuk,* Michael Nicklas, Lev Akselrud, Walter Schnelle, Ulrich Schwarz, Alexander A. Tsirlin, Andreas Leithe-Jasper, and Yuri Grin

Max-Planck-Institut für Chemische Physik fester Stoffe, Nöthnitzer Str. 40, 01187 Dresden, Germany

(Received 30 April 2013; revised manuscript received 23 May 2013; published 5 June 2013)

The intermetallic compound $Y_3Pt_4Ge_{13}$ has been synthesized by high-pressure high-temperature technique. It crystalizes with its own noncentrosymmetric type of crystal structure in the monoclinic space group Cc and is superconducting below $T_c = 4.5$ K. Thermodynamic properties as well as transport measurements were performed down to 0.4 K. The upper critical field is $\mu_0 H_{c2} = 3.8$ T, the lower one only $\mu_0 H_{c1} = 5$ mT. All observations are consistent with an s-wave symmetry single-energy gap for the superconducting phase.

DOI: 10.1103/PhysRevB.87.224502 PACS number(s): 07.35.+k, 61.05.C−, 74.70.Dd, 74.20.Fg

I. INTRODUCTION

The family of filled-skutterudite compounds MPt_4Ge_{12} with platinum-germanium framework structure comprises several members (M = Sr, Ba,[1,2] La, Pr,[1] Th[3,4]) which become superconducting. The highest critical temperature, $T_c = 8.3$ K, is observed for $LaPt_4Ge_{12}$, but, interestingly, $PrPt_4Ge_{12}$ is also a superconductor with $T_c = 7.9$ K. While the isostructural skutterudite $PrOs_4Sb_{12}$ is an unconventional heavy-fermion superconductor,[5] $PrPt_4Ge_{12}$ does not show strong electronic correlations.[1] Reports on the properties of its superconducting gap are controversial: The presence of point nodes[6] as well as time-reversal symmetry breaking[7] have been reported, while other authors suggest a conventional multigap scenario,[8–10] which has been substantiated by the results of penetration depth measurements in a recent study.[11]

Under ambient pressure, the formation of filled skutterudites MPt_4Ge_{12} has been accomplished only with the light trivalent rare-earth metals. $EuPt_4Ge_{12}$ is formed at ambient pressure, however it contains Eu in the valence state 2+. The compound $SmPt_4Ge_{12}$ could only be synthesized by application of high external pressure (≈5 GPa).[12] Since chemical equilibria, activity, and reaction kinetics can be significantly influenced by application of high pressure, the formation of novel materials can be facilitated by this approach.[13] Recently, we started an exploratory study with the aim to synthesize skutterudites with the heavier rare-earth metals and yttrium. Instead, we found that compounds with a composition $M_3Pt_4Ge_{13}$ (M = Ca, Y, Pr, Sm, Gd-Yb) form. We have shown that their crystal structures are closely related to the $Yb_3Rh_4Sn_{13}$ type of structure, however, with a variety of subtle structural distortions.[14]

Intermetallic compounds with the centrosymmetric $Yb_3Rh_4Sn_{13}$ structure type (space group $Pm\bar{3}n$) or derived variants of this type have been found in many systems A-T-X (where A are alkaline-earth, rare-earth, or actinide metals; T are transition metals of groups VIII–X; and X = In, Si, Ge, Sn or Pb).[15–18] They became an object of many studies, mostly due to the interesting interplay between magnetic and superconducting properties.[19] $Yb_3Rh_4Sn_{13}$ and $Yb_3Co_{4.3}Sn_{12.7}$ are magnetic and conventional BCS superconductors with T_c of 8.6 K[17,20] and 3.4 K,[21] respectively. The centrosymmetric cubic nonmagnetic compounds $R_3T_4Sn_{13}$ (R = La, Sr; T = Rh, Ir) are superconducting with $T_c = 2.5$–5 K, isotropic energy gap and strong electron-phonon coupling.[22] However, a recent study showed that the low-temperature structure of $Sr_3Ir_4Sn_{13}$ is noncentrosymmetric (space group $I\bar{4}3d$) with doubled unit cell parameter ($a_{cub2} \approx 2a_{cub}$).[23] Another compound of special interest is $Ca_3Ir_4Sn_{13}$, in which superconductivity with $T_c = 7$ K is claimed to coexist with ferromagnetic spin fluctuations.[24,25] Among the known $R_3T_4Ge_{13}$ compounds crystallizing with the centrosymmetric $Yb_3Rh_4Sn_{13}$ type structure, $Y_3Ru_4Ge_{13}$ and $Lu_3Ru_4Ge_{13}$ are superconducting with $T_c = 1.8$ and 2.3 K, respectively.[26,27]

Here, we report on the high-pressure high-temperature synthesis and the superconducting properties of $Y_3Pt_4Ge_{13}$, a compound with a monoclinic noncentrosymmetric crystal structure. Special attention is paid to the structural subtleties of $Y_3Pt_4Ge_{13}$ which are elaborated in detail. Most superconductors investigated up to now have simple and centrosymmetric crystal structures. In crystals lacking the inversion symmetry, the parity of the superconducting wave function has no meaning, i.e., the pairing state can not be classified as either singlet or triplet and may be of mixed character. This may lead to novel phenomena,[28] e.g., an upper critical field exceeding the Pauli limit. Due to the lack of inversion symmetry, an antisymmetric spin-orbit interaction term may lead to the splitting of electronic bands. The superconducting state has been investigated recently in several noncentrosymmetric compounds.[28–35] Many of these compounds contain heavy transition metals, notably Ir or Pt, where strong spin-orbit coupling ($\propto Z^2$) can be expected. Most remarkably, there are a few heavy-fermion superconductors without an inversion center, most notably $CePt_3Si$,[29] which is superconducting at ambient pressure. Currently, the results for superconductors without strong correlations are quite controversial.

A particulary simple antisymmetric spin-orbit interaction is of Rashba type, where space inversion symmetry is broken only in one direction.[36] Many of the tetragonal noncentrosymmetric superconductors are of this type, however, in $Y_3Pt_4Ge_{13}$ the distortions leading to the noncentrosymmetric structure are imposed on all space directions and thus the space group remains nonpolar. For such a case theoretical predictions are more complicated.[28]

II. EXPERIMENTAL

Samples with nominal composition $Y_3Pt_4Ge_{13}$ were prepared from yttrium ingots (Dr. Lamprecht, 99.5 wt.%), platinum foil (Chempur, 99.95 wt.%) and germanium

(Chempur, 99.9999 wt.%). The educts were arc-melted (mass loss <0.5%), sealed in a tantalum tube enclosed in an evacuated silica ampoule, heat treated at 700 °C for 240 h, and quenched in water. The obtained button was multiphase: The powder X-ray diffraction (XRD) pattern indicated orthorhombic $YPtGe_2$, $PtGe_2$, and elemental Ge.

Starting with this precursor, the synthesis of monoclinic $Y_3Pt_4Ge_{13}$ has been performed in an octahedral multianvil press at 8 GPa and 850 °C. The force redistribution in the press was realized by a Walker module and MgO octahedra with edge lengths of 18 mm.[37] Boron nitride crucibles were used as a sample container. Typical annealing time was 2 h followed by cooling to room temperature (after switching off the heating) before decompression. Beside the transfer of the high-pressure assembly to/from the press, all sample handlings were performed in argon-filled glove boxes [$p(O_2/H_2O)$ <1 ppm]. The ingot could be easily recovered from the crucible and proved to be stable in air.

High-resolution (HR) powder x-ray diffraction (XRD) data for structure refinement were collected at room temperature at the ID31 beamline of the European Synchrotron Radiation Facility (ESRF) ($\lambda = 0.39986$ Å, $2\theta_{max} = 34°$) on powder enclosed in a quartz capillary with an outer diameter of 0.5 mm. The signal was measured by eight scintillation detectors, each preceded by a Si (111) analyzer crystal, in the angle range $2\theta = 1$–$40°$. The *WinXpow* program package[38] was used for phase analysis. The lattice parameters were refined by least-squares fitting (program package *WinCSD*[39]).

Pieces of the ingot were embedded in conductive resin and then grinded, polished, and finished ($\frac{1}{4}$ μm diamond abrasives). The metallographic microstructures were characterized by light-optical microscopy (Zeiss Axioplan 2) and by energy-dispersive x-ray spectroscopy (EDXS) on a Jeol JSM 6610 scanning electron microscope equipped with an UltraDry EDS detector.

The magnetization was measured in a SQUID magnetometer (MPMS XL-7, Quantum Design) in external fields between $\mu_0 H = 2$ mT and 7 T and temperatures of 1.8–400 K. The electrical resistivity and the heat capacity were measured down to 0.4 K in a commercial system (PPMS, Quantum Design) using an ac resistivity bridge (LR-700, Linear Research) and the HC option of the PPMS, respectively. Electrical contacts were made with silver-filled epoxy. In addition, the heat capacity was determined from 223–523 K in a differential scanning calorimeter (DSC8500, Perkin-Elmer, 5 K min^{-1}, argon).

The electronic structure of $Y_3Pt_4Ge_{13}$ was calculated within the local-density approximation (LDA) of the density-functional theory (DFT) using the full-potential FPLO code (version 9.01-35)[40] with the basis set of local orbitals. In the scalar relativistic calculation the exchange-correlation potential by Perdew and Wang[41] was used. The k-mesh included 512 points (80 atoms in the unit cell) in the first Brillouin zone.

III. RESULTS AND DISCUSSION

A. Phase analysis

$Y_3Pt_4Ge_{13}$ as the majority phase and $YPtGe_2$ as the minority phase were identified in the X-ray powder diffraction pattern. To estimate the phase composition more precisely, the polished cuts were examined optically and by EDXS. The element mapping based on the K- and L-lines x-ray intensities shows the presence of $Y_{3.0(1)}Pt_{4.0(1)}Ge_{13.0(1)}$ (96% of the analyzed surface), $YPtGe_2$ (3%), as well as a further minority phase $PtGe_2$ (1%; not detected in the diffraction pattern).[42]

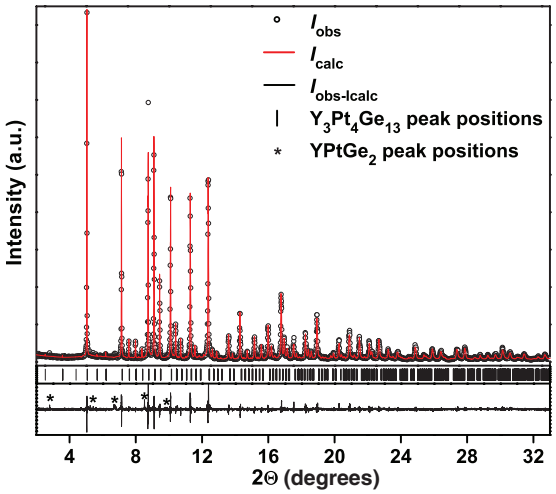

FIG. 1. (Color online) Experimental (black points) and calculated (red line) synchrotron XRD patterns of $Y_3Pt_4Ge_{13}$. Peak positions are given by black ticks; the difference plot is shown as a black line in the bottom part. Peaks excluded from the refinement ($YPtGe_2$ phase) are marked by asterisks.

B. Crystal structure

The characteristic feature of the powder XRD pattern of $Y_3Pt_4Ge_{13}$ is a pronounced grouping of the diffraction peaks around positions reflecting a cubic lattice with the parameter $a_{cub} = 9.095$ Å (Fig. 1). This lattice is similar to that of the structure type $Yb_3Rh_4Sn_{13}$,[17] which is characteristic for many compounds $RE_3TM_4Tt_{13}$ with rare-earth (RE) and transition metals (TM) with the elements of group 14 (Tt = Si, Ge, Sn),[15–18] in particular for the recently investigated germanium representatives $RE_3\{Co, Ru, Rh, Os, Ir\}_4Ge_{13}$.[15,27] However, in the diffraction pattern of $Y_3Pt_4Ge_{13}$, peaks are observed at positions which are forbidden in the cubic structure of $Yb_3Rh_4Sn_{13}$ with the space group $Pm\bar{3}n$ (cubic indexes (003) and (133), ranges II and IV in Fig. 2). This fact indicates already that the initial structural motif is distorted, and the glide symmetry plane n is suppressed. Moreover, the cubic reflection (200) (Fig. 2, range I) is split in two parts, which, after deconvolution, have the intensity ratio 1:2. With the weaker reflection having the smaller diffraction angle, this allows us to assume a tetragonal deformation of the cubic lattice with $a_{tetr} \approx a_{cub}$, $c_{tetr} \approx a_{cub}$ and $c_{tetr}/a_{tetr} < 1$. Assumption of such a lattice allows us to achieve a better indexing of the powder diffraction pattern in the ranges I, II, and IV (Fig. 2). Nevertheless, this lattice does not allow us to interpret the range III [initial cubic reflection (222)]. Splitting of the diffraction peak in this range indicates clearly a further monoclinic distortion of the initial cubic lattice according to $a_{mon} = b_{mon} \approx a_{cub}, c_{mon} \approx a_{cub}$, and $\beta \neq 90°$. This distortion can also

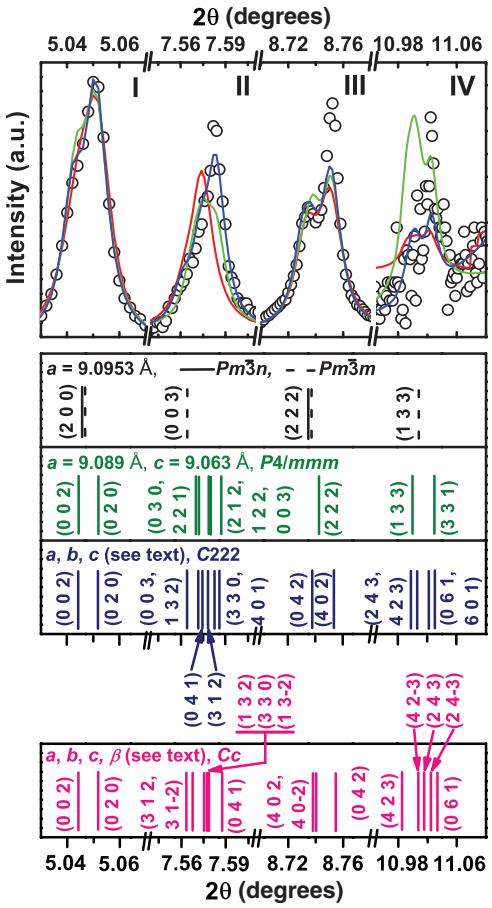

FIG. 2. (Color online) 2θ ranges 5.03–5.07° (I), 7.54–7.61° (II), 8.70–8.78° (III), and 10.95–11.10° (IV) of HR XRD pattern of $Y_3Pt_4Ge_{13}$ together with the refined profiles to the space groups $C222$ (red line), $C2/c$ (green line), and Cc (blue line) and possible indexing in space groups $Pm\bar{3}n$, $Pm\bar{3}m$, $P4/mmm$, $C222$, and Cc.

be described by the orthorhombic lattice with the unit cell of the doubled volume ($a_{orth} \approx b_{orth} \approx a_{cub}\sqrt{2}$; $c_{orth} \approx a_{cub}$). With this lattice the already visually separated reflections in the powder diffraction pattern were indexed: $a = 12.8396(2)$ Å, $b = 12.8780(2)$ Å, $c = 9.1075(2)$ Å.

However, the analysis of the extinction conditions of the observed reflection set indicated the extinction class C- - c, which is impossible in the orthorhombic symmetry.[43] Thus the extinction class was assumed to be C- - - (possible space groups $Cmmm$, $Cmm2$, $Amm2$, and $C222$). The structure solution was performed from powder diffraction data with the direct-phase-determination technique in the group $C222$. The full-profile refinement resulted in the residuals of $R_I = 0.054$ and $R_P = 0.143$ for the whole measured range.[44] Even in this group with the lowest possible symmetry, the obtained model is strongly disordered; several positions had to be split revealing local symmetry breaking. The refinement of individual displacement parameters for the majority of positions was impossible due to strong correlations within the data. In addition, the experimentally measured and calculated profiles at distinct diffraction angles differed clearly (ranges II and IV in Fig. 2). The combination of these findings with the above mentioned forbidden extinction class in the orthorhombic symmetry leads to the conclusion that the real symmetry of the crystal structure of $Y_3Pt_4Ge_{13}$ is monoclinic. The refinement of the lattice parameters confirmed this conclusion and yielded a small but relevant deviation of one of the unit cell angles from 90°: $a = 12.8781(2)$ Å, $b = 12.8381(2)$ Å, $c = 9.1081(1)$ Å, $\beta = 89.954(2)$°. First the crystal structure was solved in the centrosymmetric space group $C2/c$ also applying the direct-phase-determination technique. Further refinement resulted in large values of the reliability factors ($R_I = 0.087$ and $R_P = 0.164$) being even larger than those obtained for the orthorhombic space group $C222$.

The resulting model[45] revealed further shortcomings: (i) the crystal structure still reveals some disorder (two Ge atoms partially occupy their crystallographic sites); (ii) a strong shortening of some Ge-Ge contacts (up to 7%) is observed. Thus, the crystal structure was finally solved in the noncentrosymmetric space group Cc and refined using full-profile diffraction data to the residuals of $R_I = 0.050$ and $R_P = 0.129$ for the whole measured range. The final atomic coordinates and isotropic displacement parameters are given in Table I. The experimental and calculated synchrotron XRD patterns as well as peaks belonging to the orthorhombic $YPtGe_2$ phase (structure type $YIrGe_2$,[46] marked by asterisks) are shown in Fig. 1. Since no overlaps of these reflections with the peaks belonging to the studied $Y_3Pt_4Ge_{13}$ compound were observed, they were excluded from the refinement. The obtained model of the crystal structure is fully ordered and describes the diffraction intensity in the ranges II and IV of the powder diffraction pattern significantly better (cf. Fig. 2) than the orthorhombic and centrosymmetric one.

The same structural model was confirmed for this compound at 80 K: $a = 12.7178(2)$ Å, $b = 12.6821(2)$ Å,

TABLE I. Atomic coordinates and displacement parameters in the crystal structure of $Y_3Pt_4Ge_{13}$ at $T \approx 298$ K (space group Cc, $Z = 4$, $\rho = 8.78(1)$ g cm^{-3}).

Atom[a]	x	y	z	B_{iso}
Y1	0.0003(6)	0.0013(7)	0.0000(3)	0.53(2)
Y2	0.1214(5)	0.3732(5)	0.249(1)	0.52(2)
Y3	0.3755(6)	0.1250(5)	0.248(1)	0.53(2)
Pt1	0.0033(4)	0.2509(3)	0.4995(5)	0.29(1)
Pt2	0.0041(4)	0.2506(3)	0.0014(4)	0.27(1)
Pt3	0.2545(3)	0.5001(4)	0.0016(7)	0.25(1)
Pt4	0.2521(3)	0.0001(4)	0.0004(8)	0.27(1)
Ge1	0.7518(5)	0.2530(6)	0.256(1)	0.65(2)
Ge2	0.1684(4)	0.0139(4)	0.247(1)	0.76(2)
Ge3	0.0076(5)	0.1586(4)	0.248(1)	0.71(2)
Ge4	0.5892(6)	0.0894(6)	0.1174(7)	0.77(2)
Ge5	0.1945(6)	0.1948(5)	0.0201(7)	0.69(2)
Ge6	0.3335(7)	0.3343(6)	0.1065(6)	0.72(2)
Ge7	0.3843(7)	0.1242(6)	0.6390(6)	0.75(2)
Ge8	0.3294(7)	0.3293(7)	0.4046(6)	0.72(2)
Ge9	0.5456(4)	0.3327(4)	0.2500(2)	0.70(2)
Ge10	0.1917(6)	0.1936(5)	0.4844(7)	0.68(2)
Ge11	0.0860(6)	0.5846(6)	0.4044(7)	0.76(2)
Ge12	0.3171(5)	0.5690(4)	0.252(1)	0.68(2)
Ge13	0.4277(6)	0.0698(5)	0.9311(7)	0.72(2)

[a]All atoms are occupying a 4a crystallographic site.

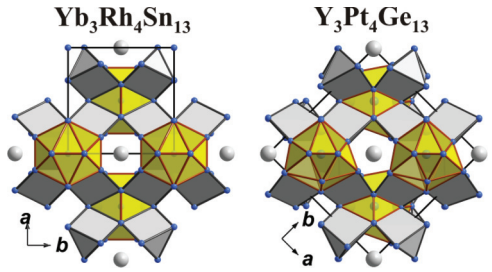

FIG. 3. (Color online) Icosahedra $Sn1Sn_{12}$ and distorted icosahedra $Ge1Ge_{12}$ (yellow) as well as trigonal prisms $RhSn_6$ and distorted trigonal prisms $PtGe_6$ (light gray) in the crystal structures of $Yb_3Rh_4Sn_{13}$ and $Y_3Pt_4Ge_{13}$ (light gray spheres—Pr or Y atoms; blue spheres—Sn or Ge atoms; Rh and Pt atoms are inside the trigonal prisms).

$c = 9.0010(1)$ Å, $\beta = 90.042(2)^{\circ}$, $V = 1451.77(6)$ Å^3, $R_I = 0.051$, and $R_P = 0.125$. However, in the DSC measurement we observed a structural phase transition for $Y_3Pt_4Ge_{13}$ with an onset temperature of 350 K and peak at 383 K. Above the transition temperature (see below), the crystal structure becomes rhombohedral (determination at 480 K). Details of the structural transition as well as the high-temperature structure will be given in a forthcoming publication.[47]

The crystal structure of $Y_3Pt_4Ge_{13}$ is closely related to the $Yb_3Rh_4Sn_{13}$ type.[17] The unit cell parameters of both structures correlate as follows: $a_{mon} \approx b_{mon} \approx a_{cub}\sqrt{2}$ and $c_{mon} \approx a_{cub}$. Both structure types show the same structural motifs of icosahedra interconnected by trigonal prisms (cf. Fig. 3). The only difference is that in $Yb_3Rh_4Sn_{13}$ icosahedra and trigonal prisms are regular, while in $Y_3Pt_4Ge_{13}$ they are distorted, similar as in recently reported $Yb_3Pt_4Ge_{13}$ and $Ca_3Pt_{4+x}Ge_{13-y}$.[14] The heavier atoms Y and Pt remain almost at the same positions as Pr and Rh atoms in the structure of the $Yb_3Rh_4Sn_{13}$ prototype, while Ge atoms are strongly shifted compared to Sn. This shift leads to the distortion of coordination polyhedra.

The interatomic distances in the crystal structure of $Y_3Pt_4Ge_{13}$ correlate mostly well with the sum of atomic radii of the elements ($r_Y = 1.81$ Å; $r_{Pt} = 1.38$ Å; $r_{Ge} = 1.23$ Å).[48] The largest contraction of 4.5% is observed for the Pt4-Ge2 contacts [$d = 2.49(1)$ Å]. The Y-Ge distances are very close to the sum of the atomic radii [3.035(9)–3.05(1) Å] and their shortening does not exceed 1%. The shortest Ge-Ge contacts in the structure of $Y_3Pt_4Ge_{13}$ are 2.508(9) Å. Finally, there are no short Pt-Pt distances in the studied compound in agreement with the $Yb_3Rh_4Sn_{13}$ prototype[17] and its derivatives $La_3Rh_4Sn_{13}$,[16] $Yb_3Pt_4Ge_{13}$, and $Ca_3Pt_{4+x}Ge_{13-y}$.[14] The coordination numbers (CN) and nearest neighbors of the Y and Pt atoms in the structure of $Y_3Pt_4Ge_{13}$ are also the same as those reported for the $Yb_3Rh_4Sn_{13}$ type. In contrast, the CNs for Ge vary between 9 and 13 due to the distortion of the Ge framework.

C. Physical properties

Measurements of the high-field magnetic susceptibility showed $Y_3Pt_4Ge_{13}$ to be diamagnetic in the whole investigated temperature range [Fig. 4(a)], with an extrapolated value of $\chi_0 \approx -367(10) \times 10^{-6}$ emu mol^{-1} at $T = 0$. $\chi(T)$

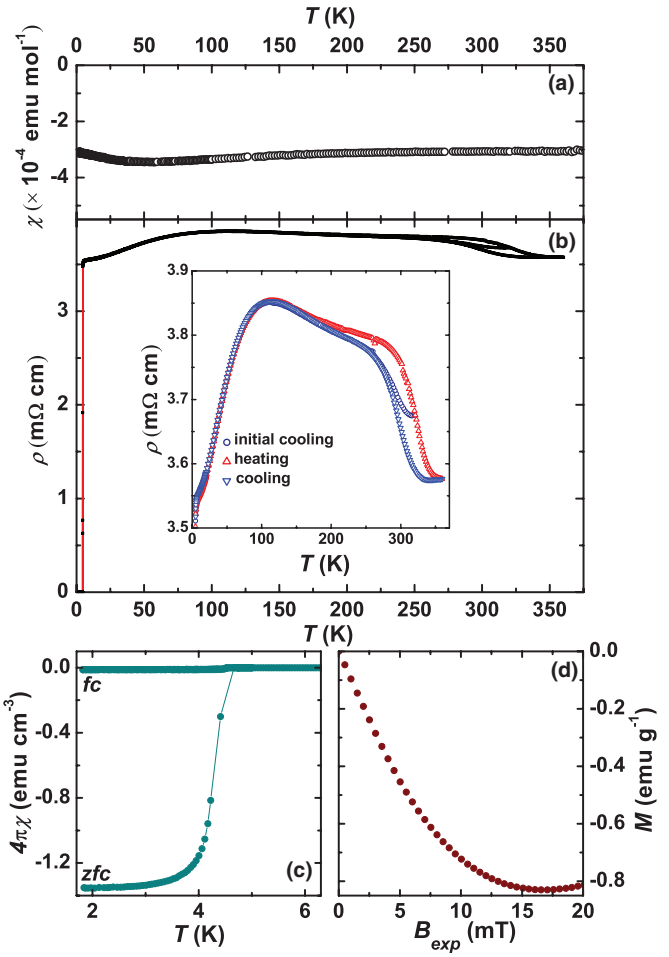

FIG. 4. (Color online) Magnetic susceptibility ($\mu_0 H = 7$ T) (a); electrical resistivity (the inset shows a magnification of the data at high temperatures) (b); magnetic susceptibility for $\mu_0 H = 2$ mT measured in zfc and fc conditions (c); and isothermal magnetization of $Y_3Pt_4Ge_{13}$ at $T = 1.85$ K for the determination of H_{c1} (d).

increases with temperature and saturates at $\approx -307(10) \times 10^{-6}$ emu mol^{-1} at $T = 400$ K. A realistic estimate of the diamagnetic contributions in metallic cage compounds is problematic due to the presence of strong additional diamagnetic terms, as, e.g., in clathrates.[49] The expected Pauli-paramagnetic contribution can therefore not be calculated. The temperature dependence of $\chi(T)$ may be due to the diamagnetic contributions or may also indicate a Pauli-paramagnetic contribution from a strongly structured electronic DOS at the Fermi level (cf., e.g., Ref. 50). Besides this, the sample contains a minor amount of Curie-paramagnetic impurities (equivalent to 0.03% of the $S = \frac{1}{2}$ species). The temperature dependence of the zero-field-cooled (zfc) and field-cooled (fc) magnetic susceptibility of $Y_3Pt_4Ge_{13}$ in a field of 2 mT is given in Fig. 4(c). A diamagnetic superconducting transition is observed at $T_c^{mag} = 4.52$ K. Considering the demagnetization correction, the diamagnetic response in zfc is close to complete. The fc signal (Meissner effect) is much weaker, which is most probably due to strong flux line pinning in this type-II superconductor.

The lower critical field $\mu_0 H_{c1}$, that is the appearance of flux lines in the sample volume, is signalled by the departure of the

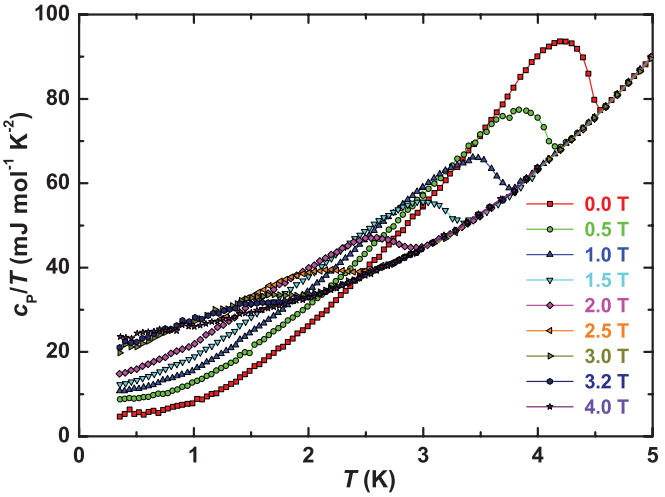

FIG. 5. (Color online) Specific heat c_p/T vs T in various magnetic fields for $Y_3Pt_4Ge_{13}$.

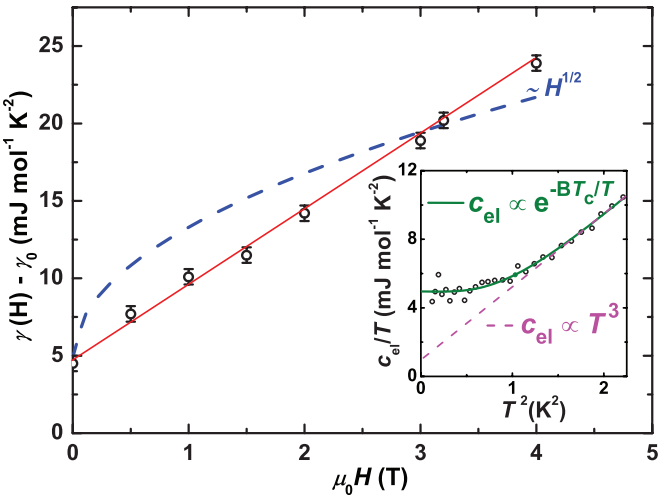

FIG. 6. (Color online) Sommerfeld parameter γ_H as a function of magnetic field $\mu_0 H$. The solid (red) line indicates a linear dependence ($\gamma_H \sim H$) typical for an s-wave gap, the dotted (blue) line represents the dependence expected for an anisotropic gap or a gap with nodes ($\gamma_H \sim H^{1/2}$). The inset shows the dependence of the electronic specific heat $c_{\rm el}$ vs T^2 together with the fits $\propto e^{-BT_c/T}$ (s-wave gap) and $\propto T^3$ (gap with nodes).

magnetization [Fig. 4(d)] from its initial linear behavior. A small rod-shaped sample was measured with the field parallel to the long axis. Adopting a criterion of 5% departure, we find $\mu_0 H_{c1} \approx 5$ mT at 1.85 K. The noise in the magnetization signal of the same sample piece at high fields was too strong to obtain a value for the upper critical field $\mu_0 H_{c2}$, which, however, can be derived from other properties (see below).

The specific heat c_p/T vs T in the temperature range 0.5–5 K and in various magnetic fields is presented in Fig. 5. A sizable but rounded steplike anomaly with an onset $T_c = 4.49$ K (consistent with $T_c^{\rm mag}$) confirms the bulk nature of the superconductivity. The observed rounding is most probably due to chemical inhomogeneities in the sample after high-pressure synthesis.[42] The second-order phase transitions for all fields were analyzed by a graphical equal-areas approximation (entropy-conserving). For zerofield, the resulting reduced "jump" $\Delta c_p/T$ and the midpoint $T_c^{\rm cal}$ are 34.2 mJ mol^{-1} K^{-2} and 4.39 K, respectively, although the jump height might be a bit overestimated by this method due to the asymmetric shape of the step.

The normal-state specific heat (data taken in a field of 5 T) is analyzed within the ansatz $c_p(T) = \gamma_N T + \beta T^3$ in the temperature range 0.5–4 K. The resulting parameters are the Sommerfeld coefficient of the electronic heat capacity $\gamma_{\rm tot} = 23.9$ mJ mol^{-1} K^{-2} and $\beta = 2.29$ mJ mol^{-1} K^{-4}, which is equivalent to a Debye temperature $\Theta_D = 257$ K.

Subtracting the βT^3 lattice term, we can analyze the electronic contribution well below T_c. The inset of Fig. 6 shows zero-field data for $c_{\rm el}/T$ vs T^2. Obviously, the electronic contribution in the superconducting state at $H = 0$ does not tend to zero but instead to $\gamma_0 = 4.9$ mJ mol^{-1} K^{-2}. This residual term is most probably due to the presence of a nonsuperconducting metallic impurity phase or of an amorphous material. Compared to $\gamma_{\rm tot}$, this large value of γ_0 suggests significant amounts of such impurities, which is in agreement with the HR-XRD phase analysis and metallographical investigations.[42]

The temperature dependence of $c_{\rm el}$ for all measured magnetic fields is well described by $\gamma_0 T + \gamma T_c A e^{-\Delta(0)/k_B T}$, as expected for a superconductor without nodes in the gap (data shown only for $H = 0$). For comparison, we also illustrate a T^3 behavior, as predicted for excitations in a gap with point nodes. The parameters from the fit for $H = 0$ are $A = 10(2)$ and $\Delta(0)/k_B T_c = 1.66(7)$. Both agree well with the values of 8.5 (temperature interval $2.5 < T_c/T < 6$)[51] and 1.76 for the weak electron-phonon coupling BCS theory.

In the main panel of Fig. 6, the Sommerfeld parameter $\gamma(H)$ extrapolated to $T = 0$, as obtained from the fits, is plotted against the field. A clear linear relation with the magnetic field is seen, which means that γ_H is simply proportional to the number of field-induced flux lines. For a superconductor with a strongly anisotropic gap or a gap with nodes, $c_{\rm el}$ is expected to be $\propto T^3$ and $\gamma(H)$ should follow a nonlinear dependence $\propto H^{1/2}$. This is not a case for the studied compound (cf. Fig. 6).

Correcting the normal state electronic specific heat coefficient by the residual term, $\gamma_N = \gamma_{\rm tot} - \gamma_0$, we obtain $\gamma_N = 19.0$ mJ mol^{-1} K^{-2}. The ratio $\Delta c_p/(\gamma_N T_c) = 1.80$ thus indicates a slightly stronger electron-phonon coupling than the weak-coupling BCS limit [$\Delta c_p/(\gamma_N T_c) = 1.43$], in contrast to the analysis of $\gamma(H)$. These discrepancies are most probably due to the imperfections of the high-pressure sample. Nevertheless, all these findings indicate that $Y_3Pt_4Ge_{13}$ is a superconductor with an s-wave gap and the electron-phonon coupling close to the BCS weak-coupling limit.

The electrical resistivity of $Y_3Pt_4Ge_{13}$ shows two phase transitions [see Fig. 4(b)]. In the high-temperature range (130–360 K), a hysteresis loop is observed, which is a clear indication of the first-order structural phase transition. This finding is also confirmed by temperature-dependent powder HR-XRD measurements that show a change in the crystal structure of $Y_3Pt_4Ge_{13}$ from monoclinic to rhombohedral with increasing T.[47] The electrical resistivity of $Y_3Pt_4Ge_{13}$ in the temperature range 5–130 K decreases with decreasing T and is reminiscent of a simple metal. However, its values are very high [$\rho(5\ {\rm K}) = 3.52$ mΩ cm] and well above the

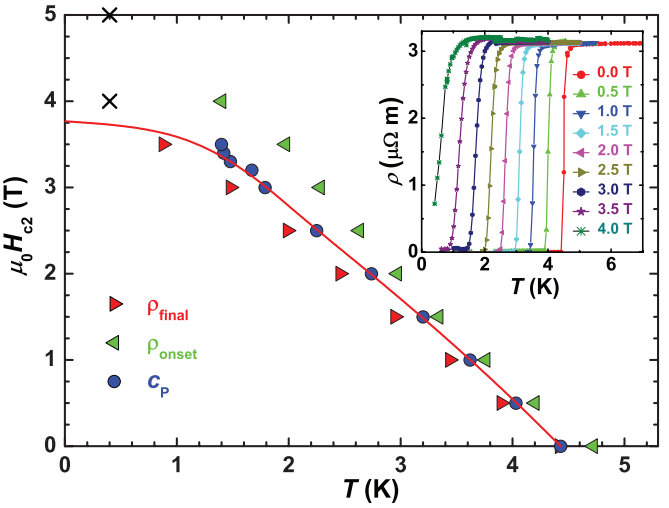

FIG. 7. (Color online) Upper critical field $\mu_0 H_{c2}$ of $Y_3Pt_4Ge_{13}$ vs temperature determined from electrical resistivity and specific heat measurements. Symbol (×) means no superconducting transition above 0.4 K. Inset: Electrical resistivity of $Y_3Pt_4Ge_{13}$ in magnetic fields up to $\mu_0 H = 4$ T.

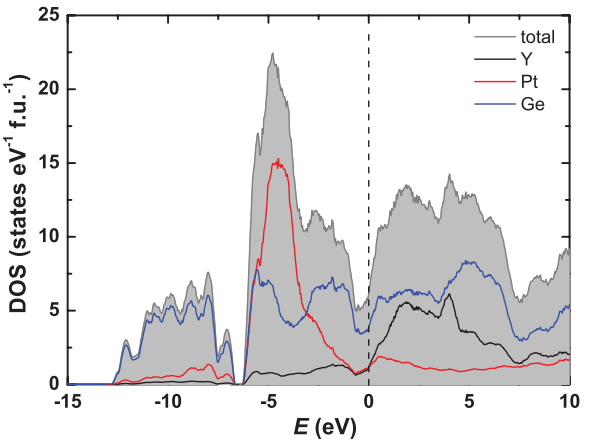

FIG. 8. (Color online) Calculated electronic density of states (DOS) for $Y_3Pt_4Ge_{13}$. The Fermi level is indicated by the dashed line.

Mott-Ioffe-Regel limit (∼0.1 mΩ cm). Similar behavior of $\rho(T)$ was reported recently for $Yb_3Pt_4Ge_{13}$.[14] Finally, at $T_c = 4.60$ K the resistivity of $Y_3Pt_4Ge_{13}$ shows the superconducting transition.

The inset of Fig. 7 presents the magnetic field dependence of the electrical resistivity of $Y_3Pt_4Ge_{13}$ at the superconducting transition. As in the case of specific heat, the observed transitions are broad. The midpoint of the resistive transition under zero field is at $T_c^{\rm mid} = 4.60$ K. Increasing magnetic fields leads to a continuous lowering of T_c, and for $\mu_0 H \geqslant 4$ T no sign of superconductivity is observed at temperatures above 0.4 K. For the determination of the upper critical field H_{c2}, the temperature points of the zero resistance, the resistive transition onset, as well as the midpoint temperatures of the jumps in $c_p(T,H)$ are plotted in Fig. 7. Interestingly, all the curves vary linearly with H down to $0.3T_c$. A free extrapolation (red line in Fig. 7) leads to the estimate for the upper critical field, $\mu_0 H_{c2}(0) \approx 3.8$ T. This corresponds to a Ginzburg-Landau coherence length $\xi_{\rm GL}(0) = 233$ Å as calculated from $\mu_0 H_{c2} = \Phi_0/2\pi\xi_{\rm GL}^2$ (Φ_0 is the flux quantum $h/2e$). $H_{c2}(0)$ is significantly lower than the Pauli-paramagnetic limit for weak electron-phonon coupling, $\mu_0 H_{c2}^p$[Tesla] = $1.86T_c$[Kelvin].[52,53]

Our studies of the transport and thermodynamic properties of $Y_3Pt_4Ge_{13}$ indicate a single s-wave gap and an upper critical field significantly lower than the Pauli limit. It should be noted that a similar situation is observed in the noncentrosymmetric superconductor $Mg_{10}Ir_{19}B_{16}$.[32] However, in some systems with multiple superconducting gaps the true nature of the superconducting state could not be elucidated in thermodynamic data at all. Therefore, to finally clarify the nature of the superconducting state of $Y_3Pt_4Ge_{13}$ some complementary studies (e.g., μSR spectroscopy, high-precision penetration depth measurements, point-contact spectroscopy, etc.) are desirable.

D. Electronic structure

Figure 8 shows the calculated electronic density of states (DOS) for $Y_3Pt_4Ge_{13}$. The energetically low-lying states between −13 and −7 eV are due to the mixing of Ge 4p and 4s with the small contribution of the Pt 5d states. The region at higher energies -7 eV $\leqslant E \leqslant E_F$ is dominated by Ge 4p, Pt 5d, and Y 4d states. Pt 5d states form a narrow complex of an approximately 3 eV bandwidth centered at about −4 eV similar to that reported for the platinum germanium filled skutterudites[1,54] and $\{Ca,Yb\}_3Pt_4Ge_{13}$.[14] The Fermi level is located close to a dip of the DOS. The DOS at E_F is predominantly composed of Ge 4p states with a small admixture of Pt 5d states. In principle, fully relativistic calculations would be important to analyze the bands split by antisymmetric spin-orbit interactions in a noncentrosymmetric compound with 5d elements.[28] Such calculations, however, are rather difficult because of the large unit cell of the present compound. However, the contribution of Pt bands at E_F is quite small, hence no strong changes of the DOS at E_F should be expected. In the scalar-relativistic calculation, we find $N(E_F) = 6.4$ states eV^{-1} f.u.$^{-1}$, which results in a bare Sommerfeld coefficient of the electronic specific heat $\gamma_{\rm bare} = 15.1$ mJ mol^{-1} K^{-2}. This implies a moderate mass enhancement of ≈1.3 compared to the experimental $\gamma_N = 19$ mJ mol^{-1} K^{-2}.

IV. CONCLUSIONS

$Y_3Pt_4Ge_{13}$, a derivative of the $Yb_3Rh_4Sn_{13}$ type, with the monoclinic noncentrosymmetric crystal structure, has been synthesized using a high-pressure high-temperature technique (8 GPa, 850 °C). Magnetic susceptibility, electrical resistivity, and specific heat measurements show a superconducting transition at $T_c = 4.5$ K. The analysis of transport and thermodynamic measurements identify $Y_3Pt_4Ge_{13}$ as a conventional BCS superconductor, with the ratio $\Delta c_p/(\gamma_N T_c) \approx 1.8$ (with slightly stronger electron-phonon coupling) and the energy gap ratio $\Delta(0)/k_B T_c = 1.66(7)$ K, which indicates a single s-wave gap. However, for a final classification of the superconducting state, complemental studies are desirable.

ACKNOWLEDGMENTS

The authors thank M. Schöneich and S. Leipe for their assistance during the high-pressure syntheses. We acknowledge ESRF for granting the beam time at ID31 and thank C. Curfs for her kind support during the high-resolution XRD measurements. We are grateful to H. Borrmann for performing powder diffraction measurements and U. Burkhardt, P. Scheppan, and S. Kostmann for the metallographical analysis. We also thank H. Rosner for discussions.

*roman.gumeniuk@cpfs.mpg.de

[1] R. Gumeniuk, W. Schnelle, H. Rosner, M. Nicklas, A. Leithe-Jasper, and Y. Grin, Phys. Rev. Lett. **100**, 017002 (2008).
[2] E. Bauer *et al.*, Phys. Rev. Lett. **99**, 217001 (2007).
[3] D. Kaczorowski and V. H. Tran, Phys. Rev. B **77**, 180504 (2008).
[4] E. Bauer, X.-Q. Chen, P. Rogl, G. Hilscher, H. Michor, E. Royanian, R. Podloucky, G. Giester, O. Sologub, and A. P. Goncalves, Phys. Rev. B **78**, 064516 (2008).
[5] H. Sato, H. Sugawara, Y. Aoki, and H. Harima, in *Handbook of Magnetic Materials*, edited by K. H. J. Buschow, Vol. 18 (Elsevier, Amsterdam, 2009).
[6] A. Maisuradze, M. Nicklas, R. Gumeniuk, C. Baines, W. Schnelle, H. Rosner, A. Leithe-Jasper, Y. Grin, and R. Khasanov, Phys. Rev. Lett. **103**, 147002 (2009).
[7] A. Maisuradze, W. Schnelle, R. Khasanov, R. Gumeniuk, M. Nicklas, H. Rosner, A. Leithe-Jasper, Y. Grin, A. Amato, and P. Thalmeier, Phys. Rev. B **82**, 024524 (2010).
[8] M. Toda, H. Sugawara, K. Magishi, T. Saito, K. Koyama, Y. Aoki, and H. Sato, J. Phys. Soc. Jpn. **77**, 124702 (2008).
[9] Y. Nakamura, H. Okazaki, R. Yoshida, T. Wakita, H. Takeya, K. Hirata, M. Hirai, Y. Muraoka, and T. Yokoya, Phys. Rev. B **86**, 014521 (2012).
[10] L. S. S. Chandra, M. K. Chattopadhyay, and S. B. Roy, Phil. Mag. **92**, 3866 (2012).
[11] J. L. Zhang *et al.*, Phys. Rev. B **87**, 064502 (2013).
[12] R. Gumeniuk *et al.*, New J. Phys. **12**, 103035 (2010).
[13] J. Bedding, Annu. Rev. Mater. Sci. **28**, 631 (1998).
[14] R. Gumeniuk *et al.*, Dalton Trans. **41**, 6299 (2012).
[15] P. Villars, *Pearson's Handbook, Crystallographic Data for Intermetallic Phases* (Materials Park, OH, 1997).
[16] P. Bordet, D. Cox, G. Espinosa, J. Hodeau, and M. Marezio, Solid State Commun. **78**, 359 (1991).
[17] J. Hodeau, J. Chenavas, M. Marezio, and J. Remeika, Solid State Commun. **36**, 839 (1980).
[18] J. Vandenberg, Mater. Res. Bull. **15**, 835 (1980).
[19] G. Shenoy, B. Dunlap, and F. Fradin, *Ternary superconductors* (Elsevier-North-Holland, Amsterdam, 1981).
[20] J. Remeika *et al.*, Solid State Commun. **34**, 923 (1980).
[21] Y. Mudryk *et al.*, J. Phys.: Condens. Matter **13**, 7391 (2001).
[22] N. Kase, H. Hayamizu, and J. Akimitsu, Phys. Rev. B **83**, 184509 (2011).
[23] L. E. Klintberg, S. K. Goh, P. L. Alireza, P. J. Saines, D. A. Tompsett, P. W. Logg, J. Yang, B. Chen, K. Yoshimura, and F. M. Grosche, Phys. Rev. Lett. **109**, 237008 (2012).
[24] J. Yang, B. Chen, C. Michioka, and K. Yoshimura, J. Phys. Soc. Jpn. **79**, 113705 (2010).
[25] S. Y. Zhou, H. Zhang, X. C. Hong, B. Y. Pan, X. Qiu, W. N. Dong, X. L. Li, and S. Y. Li, Phys. Rev. B **86**, 064504 (2012).
[26] C. K. Segre, H. F. Braun, and K. Yvon, in *Ternary Supercond. Proc. Int. Conf.*, edited by G. K. Shenoy, B. D. Dunlop, and F. Y. Fradin (Elsevier-North-Holland, Amsterdam, 1981), pp. 243–246.
[27] K. Ghosh, S. Ramakrishnan, and G. Chandra, Phys. Rev. B **48**, 10435 (1993).
[28] *Non-centrosymmetric Superconductors*, edited by E. Bauer and M. Sigrist (Springer, Berlin Heidelberg, 2012).
[29] E. Bauer, G. Hilscher, H. Michor, C. Paul, E. W. Scheidt, A. Gribanov, Y. Seropegin, H. Noël, M. Sigrist, and P. Rogl, Phys. Rev. Lett. **92**, 027003 (2004).
[30] I. Sugitani *et al.*, J. Phys. Soc. Jpn. **75**, 043703 (2006).
[31] H. Q. Yuan, D. F. Agterberg, N. Hayashi, P. Badica, D. Vandervelde, K. Togano, M. Sigrist, and M. B. Salamon, Phys. Rev. Lett. **97**, 017006 (2006).
[32] T. Klimczuk, F. Ronning, V. Sidorov, R. J. Cava, and J. D. Thompson, Phys. Rev. Lett. **99**, 257004 (2007).
[33] E. Bauer *et al.*, Phys. Rev. B **80**, 064504 (2009).
[34] G. Eguchi, D. C. Peets, M. Kriener, Y. Maeno, E. Nishibori, Y. Kumazawa, K. Banno, S. Maki, and H. Sawa, Phys. Rev. B **83**, 024512 (2011).
[35] K. Miliyanchuk *et al.*, J. Phys.: Conf. Series **273**, 012078 (2011).
[36] L. P. Gor'kov and E. I. Rashba, Phys. Rev. Lett. **87**, 037004 (2001).
[37] D. Walker, M. Carpenter, and C. Hitch, Am. Mineral. **75**, 1020 (1990).
[38] STOE Powder Diffraction Software, WinXPow (version 2), Darmstadt, STOE and Cie GmbH, 2001.
[39] L. Akselrud, P. Zavalii, Y. Grin, V. Pecharsky, B. Baumgartner, and E. Wölfel, Mater. Sci. Forum **133-136**, 335 (1993).
[40] K. Koepernik and H. Eschrig, Phys. Rev. B **59**, 1743 (1999).
[41] J. P. Perdew and Y. Wang, Phys. Rev. B **45**, 13244 (1992).
[42] The method also has its specific drawbacks: Even small pressure and temperature gradients in the press inevitably lead to chemical inhomogeneities or even multiphase samples. A true optimization of the synthetic parameters is a very tedious task. Also, materials which are metastable at ambient pressure cannot be annealed in order to reduce mechanical stress and to enhance the chemical homogeneity.
[43] T. Hahn, *International Tables for Crystallography* (Kluwer Academic Publishers, Dordrecht-Boston-London, 1996).
[44] Space group $C222$; $a = 12.8396(2)$ Å, $b = 12.8780(2)$ Å, $c = 9.1075(2)$ Å; $R_I = 0.054$ and $R_P = 0.143$; Y1 in 2*b* (1/2 0 0); Y2 in 2*c* (1/2 0 1/2), $G = 0.89(1)$; Y3 in 8*l* (0.1234(3) 0.1222(4) 0.2481(7)), $G = 0.93(1)$; Y4 in 8*l* (0.534(2) −0.017(2) 0.324(2)), $G = 0.14(1)$; Pt1 in 4*e* (0.2485(3) 0 0), $G = 0.87(1)$; Pt2 in 4*f* (0.2482(3) 0 1/2); Pt3 in 4*g* (1/2 0.2488(2) 0); Pt4 in 4*h* (1/2 0.2448(2) 1/2); Ge1 in 4*k* (1/4 3/4 0.2599(8)), $G = 0.86(1)$; Ge2 in 4*e* (0.094(4) 0 0), $G = 0.11(1)$; Ge3 in 8*l* (0.0860(7) 0.0710(7) 0.919(1)), $G = 0.57(1)$; Ge4 in 8*l* (0.1102(8) 0.1151(1) 0.652(1), $G = 0.45(1)$); Ge5 in 8*l* (0.3370(3) 0.0129(4) 0.7518(8)); Ge6 in 8*l* (0.3022(4) 0.1850(5) 0.4468(6)), $G = 0.84(1)$; Ge7 in 8*l* (0.3362(4) 0.1695(5) 0.1110(6)), $G = 0.84(1)$; Ge8 in 8*l* (0.0620(4) 0.3125(5) 0.752(1), $G = 0.74(1)$; Ge9 in 8*l* (0.8682(9) 0.120(1) 0.137(1)), $G = 0.44(1)$; Ge10 in 8*l* (0.9318(6) 0.0729(7) 0.425(1)), $G = 0.59(1)$; Ge11 in 8*l* (0.687(1) 0.189(1) 0.9989(1)),

$G = 0.35(1)$. $B_{iso} = 0.65$ for all atoms and were fixed during the refinement.

[45]Space group $C2/c$; $a = 12.8795(2)$ Å, $b = 12.8389(2)$ Å, $c = 9.1073(2)$ Å$R_I = 0.087$ and $R_P = 0.164$; Y1 in $4e$ (1/2 0.001(1) 1/4), $B_{iso} = 0.76(1)$; Y2 in $8f$ (0.1217(9) 0.8745(8) 0.002(1)), $B_{iso} = 0.68(1)$; Pt1 in $4e$ (0 0.7510(5) 1/4) $B_{iso} = 0.23(1)$; Pt2 in $4e$ (0 0.2532(4) 1/4), $B_{iso} = 0.301(8)$; Pt3 in $8f$ 0.7479(4) 0.0019(3) 0.2452(4), $B_{iso} = 0.202(8)$; Ge1 in $4c$ (3/4 1/4 1/2), $B_{iso} = 0.838(9)$; Ge2 in $8f$ (0.9223(9) 0.0679(7) 0.326(1)), $B_{iso} = 0.90(1)$; Ge3 in $8f$ (0.125(1) 0.8751(9) 0.3950(9)), $B_{iso} = 0.943(9)$; Ge4 in $8f$ (0.1898(9) 0.3157(8) 0.731(1)), $G = 0.78(1)$, $B_{iso} = 1.106(9)$; Ge5 in $8f$ (0.8169(9) 0.6905(8) 0.693(1)), $B_{iso} = 0.99(1)$; Ge6 in $8f$ (0.6606(7) 0.9896(8) 0.002(2)), $G = 0.87(2)$, $B_{iso} = 1.06(1)$; Ge7 in $8f$ (0.503(1) 0.8413(6) 0.000(1)), $B_{iso} = 0.97(1)$.

[46]M. François, G. Venturini, E. McRae, B. Malaman, and B. Roques, J. Less-Common Met. **128**, 249 (1987).

[47]R. Gumeniuk (unpublished).

[48]J. Emsley, *The Elements* (Oxford University Press, New York, 1998).

[49]C. Cros, M. Pouchard, and P. Hagenmuller, J. Solid State Chem. **2**, 570 (1970).

[50]R. Gumeniuk, H. Rosner, W. Schnelle, M. Nicklas, A. Leithe-Jasper, and Y. Grin, Phys. Rev. B **82**, 052504 (2008).

[51]A. Tari, *The Specific Heat of Matter at Low Temperatures* (Imperial College Press, London, 2003).

[52]A. M. Clogston, Phys. Rev. Lett. **9**, 226 (1962).

[53]B. S. Chandrasekhar, J. Appl. Phys. Lett. **1**, 7 (1962).

[54]H. Rosner *et al.*, Phys. Rev. B **80**, 075114 (2009).